

Article

Ensuring the Abrasive Jet Machining Efficiency Using a Nozzle with a Perforated Insert

Vadym Baha ¹, Ivan Pavlenko ^{2,3,*} , Kamil Židek ³  and Olaf Ciszak ⁴ 

¹ Department of Technical Thermal Physics, Sumy State University, 116, Kharkivska St., 40007 Sumy, Ukraine; v.baga@kttf.sumdu.edu.ua

² Department of Computational Mechanics Named after Volodymyr Martynovskyy, Sumy State University, 116, Kharkivska St., 40007 Sumy, Ukraine

³ Department of Industrial Engineering and Informatics, Technical University of Košice, 1, Bayerova St., 080 01 Prešov, Slovakia; kamil.zidek@tuke.sk

⁴ Faculty of Mechanical Engineering, Poznan University of Technology, 2, Piotrowo St., 61-138 Poznan, Poland; olaf.ciszak@put.poznan.pl

* Correspondence: i.pavlenko@cm.sumdu.edu.ua

Abstract: Ejector-cleaning devices for abrasive jet machining have various practical applications. The working nozzle is one of the device's key elements affecting the treated surface quality. There arises the necessity for new approaches to achieving an efficiency increase in abrasive jet equipment nozzles, namely their design improvement and further development of a new, relatively cheap but effective technology for their manufacturing and maintenance. This technology should allow for the high durability of nozzles without being essential for the hardness or wear resistance parameters of the material used for manufacturing. The nozzle should be designed as a long-length perforated insert to allow for radial airflow, forcing the abrasive material (river sand) from the inner walls of the nozzle's working surface to reduce its friction with the abrasive material. This will result in new wear-out conditions, providing an essential decrease in the wear-out of a nozzle's working surface. The article aims to develop a more effective design for the working nozzle based on the perforated insert application. The task was set to provide a more detailed experimental and theoretical study of the processes in perforated nozzles to improve their effectiveness. The research resulted in a new design for nozzles with higher efficiency.

Keywords: machining; Venturi nozzle; process innovation; flow ratio; process intensification



Citation: Baha, V.; Pavlenko, I.; Židek, K.; Ciszak, O. Ensuring the Abrasive Jet Machining Efficiency Using a Nozzle with a Perforated Insert. *Machines* **2024**, *12*, 347. <https://doi.org/10.3390/machines12050347>

Academic Editor: Kai Cheng

Received: 16 April 2024

Revised: 15 May 2024

Accepted: 16 May 2024

Published: 16 May 2024



Copyright: © 2024 by the authors. Licensee MDPI, Basel, Switzerland. This article is an open access article distributed under the terms and conditions of the Creative Commons Attribution (CC BY) license (<https://creativecommons.org/licenses/by/4.0/>).

1. Introduction

Developing new and more effective working nozzle designs is topical for modernizing the devices for abrasive jet machining [1]. The primary factors that determine the effectiveness of abrasive jet machining are the following: proper abrasive-content flow dosing; the full provision of the unit with a source of compressed air (3.0–3.5 m³/min); the formation of an abrasive-air mixed flow with a maximum rate at the outlet. The first factor deals with the design and flow control valve sensibility. The second factor depends on the proper choice of a compressor station capable of satisfying the device's peak load. The efficiency of the working nozzle determines the third key factor and thus comprises the subject of our research.

The nozzles currently available for sale are expensive, though effective, due to the application of wear-resistant materials. However, their high cost has caused the shift to cheap analogs commonly made of steel which become worn crucially with time. Notably, the process of the nozzle wear leads to a significant increase in air and abrasive material consumption, and, as a result, an extra source of compressed air appears to be needed to provide the unit proper operation. If cleaning is performed in the open air, it causes extra irreversible losses of costly abrasive material.

Thus, the necessity for developing a rational design of the working nozzle that can compete in the current market becomes evident.

The primary indicator of the working nozzle efficiency of abrasive jet machining is the flow rate value of the abrasive–air mixture at its outlet. This flow rate depends on the geometrical and operating parameters of the nozzle itself. The nozzle's geometry directly impacts the distribution of the workflow rate, as well as its pressure, temperature, and density. The nozzle's internal losses are caused by friction increase against its walls due to abrasive particles' content. Therefore, an increase in nozzle efficiency is possible by applying the optimal geometry for its flow part and internal friction reduction. Both approaches should be undertaken simultaneously to achieve the maximum effect.

An efficiency increase due to finding an optimal flow profile is essential. The capture coefficient increases by 8.1–19.2% compared to a conventional ejector under the same working conditions [2]. The Venturi nozzle achieves four to seven times more aeration performance than circular nozzles [3]. In the paper [4], the capture factor, which can be used as a parameter to present the steam ejector performance, is calculated as the mass of the trapped steam working flow divided by the mass flow rate of the driving flow.

In the paper [5], the verification of the two-phase model simulation CFD was performed within the admissible discrepancies range. As a result, a positive effect was gained (up to 30%) due to nozzle geometry optimization.

Therefore, the significance of the impact of the nozzle geometry on its expendable features was proved. In the paper [6], the nozzle erosion in the well was studied. This phenomenon is similar to the jet abrasive nozzle's wear during operation. It was established that the particle size and mass flow rate are the basic factors that impact the nozzle's erosion effect and that the installation position affects the nozzle's erosion efficiency.

It should be emphasized that we experimentally established that an abrasive nozzle's wear depends on the angle of the material processed. In the paper [7], the process of microabrasive cleaning was investigated. It was established that such variables as the particle type, nozzle diameter, pressure, distance, and processing time affect the surface roughness. The paper [8] found that sand grains in the nozzle contribute to cavitation flow development, and the concentration range decreases with an increase in the average diameter. As a result, the influence of nozzle diameter on the formation of a flowing jet was shown.

The numerical simulation of the internal structure of the steam ejector in the jet cooling system was performed [9]. As a result, a numerical modeling technique was presented, and the results' correctness was shown.

Much attention was given to the methodology of the visualization of numerical results of the flow in the labyrinth seal. They were shown using color-indicated shading for the pressure, density, and velocity magnitude. Based on the ANSYS CFX v.19 software, the numerical solution method of the equation system, which presents the most generalized case of the carrier medium flow (Navier–Stokes and continuity equations), was used [10].

In [11], it was established that the nozzle neck diameter is a crucial factor affecting the ejector performance, shock wave, and internal flow structure. The paper [12] presents the study results of the geometrical characteristics of multistage steam jet ejectors. The results showed the influence of rheometric characteristics on the efficiency of the ejector.

The paper [13] described developing and testing the working nozzle with a porous insert. This made it possible to increase the efficiency of the material processing significantly.

All the abovementioned factors make it clear that a nozzle's efficiency depends on its geometry, and the wear resistance depends on the material. The task was to develop a cheaper nozzle design without a decrease in energy efficiency. Thus, there is one way left to increase the efficiency of the working nozzles of the abrasive jet units, namely to affect their geometric parameters and operation modes.

The research aims to develop a more efficient working nozzle design due to the application of perforated nozzle inserts. In our research, the application of the long-length perforated insert is proposed but not for some part of its length. To achieve the set goal, a

series of numerical and experimental studies of the operating and geometrical parameters of the working nozzle should be carried out. The results should also be analyzed.

2. Materials and Methods

2.1. Mass Flow Rate Calculations

The considered working nozzle with a porous insert is presented in Figure 1.

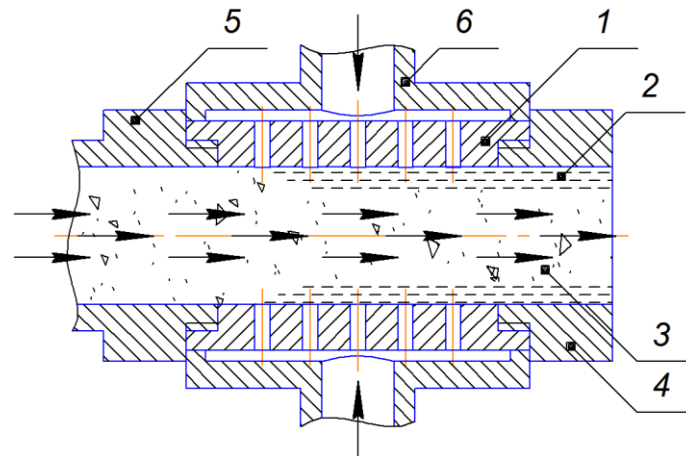


Figure 1. The design scheme of the air layer formation on the nozzle's inner surface: 1—cylindrical perforated nozzle insert; 2—air layer; 3—air-abrasive flow; 4—nozzle holder nut; 5—abrasive supply fitting; 6—air supply fitting.

Figure 1 is a conventional design scheme of the air layer organization. The nozzle with perforated insert 1 is inserted into the nozzle holder and clamped with nut 4.

The supply air pressure has a more significant effect than the number of holes. The pressure should be such that it does not affect the core of the jet but only creates a boundary air layer, pushing abrasive particles (river sand) from the nozzle's walls.

The diameter varied in the range of $d = 2\text{--}14$ mm; the length varied in the range of $l = 22\text{--}44$ mm.

River sand of an average grain size of (0.50 ± 0.05) mm was used, with a density of (1600 ± 100) kg/m³ and a melting point of about 1730 °C.

According to the available recommendations [14], the specific geometrical factor varies in a range of $\mu = 1.0\text{--}1.5$.

Due to the lack of a single systemized theoretical study on the complex flow mechanism of the air–abrasive mixture, the fundamental Stodola's formula [15] was proposed to evaluate the flow ratio through a hole with sharp edges, which was supplemented with experimental coefficients considering the peculiarities of the abrasive flow:

$$\dot{m} = \mu f K \sqrt{\frac{\rho_1}{z p_1} (p_1^2 - p_2^2)}, \quad (1)$$

where \dot{m} —the mass flow rate of the air–abrasive mixture, kg/s; μ —the nozzle's flow ratio; f —the cross-sectional area, m²; K —the nozzle flow coefficient; ρ_1 —the inlet density of a mixture, kg/m³; z —the number of holes; p_1, p_2 —the inlet and outlet pressure, respectively, Pa.

The approaches to calculating and designing nozzle elements with a relatively small cross-section (i.e., cylindrical and conical nozzles and holes with sharp edges) are based on the generalized experimental data. For example, for the labyrinth seal case study, the design is represented as a series of sequentially installed z holes with sharp edges. In this case, the flow ratio μ is also introduced to consider all the available simplifications and discrepancies [16]. Such a principle has been chosen to be applied to evaluate the flow ratio through an abrasive jet nozzle.

A perforated insert element with a permeability of 50% was used. It was manufactured from pressed metal chips with 0.5–1.0 mm holes that depend on the size of the abrasive particle used in practice during abrasive jet machining. Particularly, in this research, a material with an average diameter of 0.5 mm was used. The spent sand was sifted and reused with the addition of new sand to replace the lost part (20% on average).

The following formula determines the air consumption through the perforated insert, in m^3/s :

$$Q = \frac{V}{t}, \quad (2)$$

where V —the volume of the compressed air leakage from the air receiver, m^3 ; t —time, s.

2.2. Numerical Simulation Technique

Numerical simulations were performed to establish the impact of the nozzle diameter d on the actual and theoretical values of the mass flow rate. Numerical studies of the cylindrical nozzle flow channel with the diameter d and the length l (Figure 1) were carried out using FlowVision v.2.5.3 and ANSYS CFX v.19 software. The flow model considered fully compressible fluid with two-phase medium activation (“particle option”). Commonly, abrasive particles have diameters in the range of 0.1–1.0 mm. Therefore, in the research, a material with an average diameter of 0.5 mm was used. An implicit calculation scheme was applied.

The numerical simulation stages are presented in Figure 2.



Figure 2. The numerical simulation stages.

A series of simulations using a calculation mesh with different numbers of cells was carried out to identify the proper mesh selection. As a result, the calculation mesh with $1.1 \cdot 10^5$ cells was chosen (Figure 3).

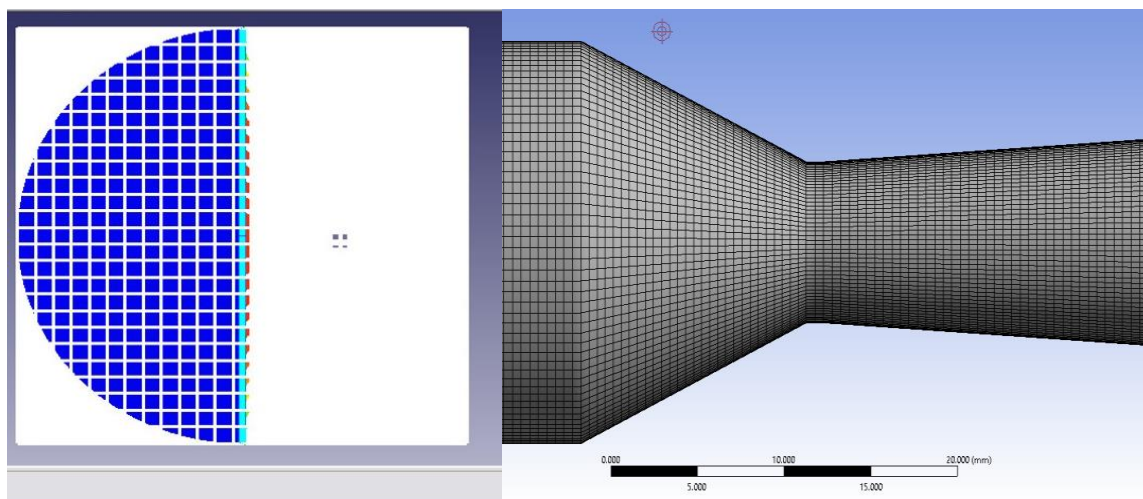


Figure 3. The calculation mesh.

The turbulent flow simulation was carried out using the Reynolds equations application and a number of turbulence models as closing equations. The flow was calculated for stationary conditions. The carrier medium was air; the abrasive material was sand, with an average size of about 0.5 mm. The flow mode was turbulent.

During the CFD simulations, the abrasive material was modeled by using spherical particles with an average diameter of 0.5 mm. The heat exchange between the sand, air, and nozzle walls was not considered.

The following turbulence models are mainly considered to solve similar problems: the “Standard” Menter SST two-equation model [17], the standard k - ε turbulence model [18], the Spalart–Allmaras turbulence model, and others [19].

The numerical results were verified through a series of experimental studies. Since comparative calculations did not demonstrate any significant discrepancies between these models, the standard k - ε model was chosen for further analysis because it agrees with most studies on gas flow. When this model is used, the system of equations for the airflow is supplemented by the following governing equations, which describe the transfer of the turbulent kinetic energy and the dissipation energy, respectively [20]:

$$\frac{\partial(\rho k)}{\partial t} + \frac{\partial(\rho \bar{u}_j k)}{\partial x_j} = \frac{\partial}{\partial x_j} \left(\frac{\mu_t}{\sigma_k} \frac{\partial k}{\partial x_j} \right) + P_k - \rho \varepsilon; \quad (3)$$

$$\frac{\partial(\rho \varepsilon)}{\partial t} + \frac{\partial(\rho \bar{u}_j \varepsilon)}{\partial x_j} = \frac{\partial}{\partial x_j} \left(\frac{\mu_t}{\sigma_\varepsilon} \frac{\partial \varepsilon}{\partial x_j} \right) + \frac{\varepsilon}{k} (C_{\varepsilon 1} P_k - \rho C_{\varepsilon 2} \varepsilon), \quad (4)$$

where t —time, s; ρ —density, kg/m^3 ; j —the number of a coordinate axis; x_j —the j -th coordinate, m; \bar{u}_j —the averaged velocity component in the j -th direction, m/s; k —the turbulent kinetic energy, m^2/s^2 ; ε —the dissipation energy, m^2/s^3 ; P_k —the production rate, $\text{kg}/(\text{m}\cdot\text{s}^3)$; μ_t —the Eddy viscosity, $\text{Pa}\cdot\text{s}$; $\sigma_k = 1.0$, $\sigma_\varepsilon = 1.3$, $C_{\varepsilon 1} = 1.44$, $C_{\varepsilon 2} = 1.92$ —the adjustable constants.

The models of particles and fully compressible fluid operate jointly since the mutual impact of two phases is assumed as follows. The carrier phase determines the particle trajectories, which, in turn, affect the flow through the mass, momentum, and energy conservation laws. The pressure drop signifies that the abrasive jet machining has entered the operation mode.

The following assumptions were made while performing the numerical studies: the flow incoming to the computational domain is axisymmetric, and the abrasive material has no moisture content.

2.3. Experimental Setup

To determine a more efficient nozzle design, a series of additional numerical studies of a cylindrical nozzle were performed considering the peculiarities of the air–abrasive mixture flow in the nozzles with different geometries (Figure 4).

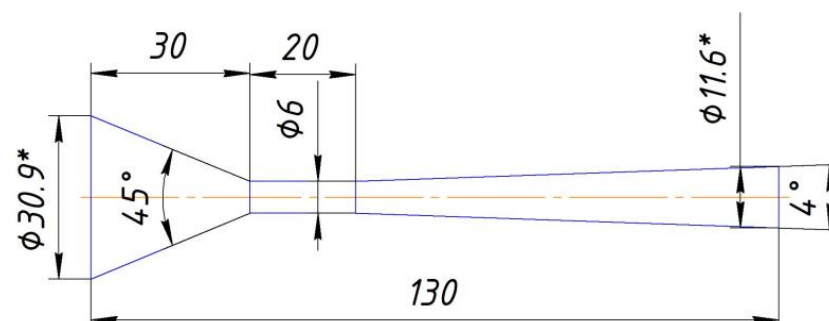


Figure 4. The cross-section of the Venturi nozzle of the abrasive jet unit (* reference dimensions).

The experimental unit is presented in Figure 5.

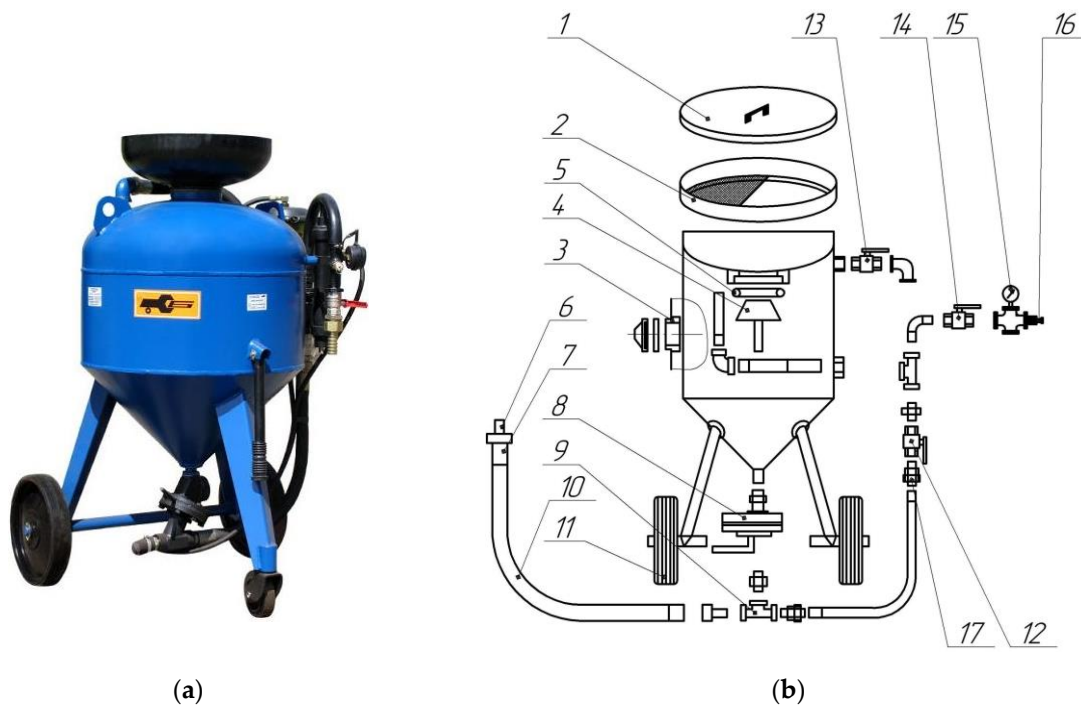


Figure 5. The experimental setup (a) and its design scheme (b): 1—cover; 2—sieve; 3—hatch; 4—closing cone; 5—closing ring; 6—abrasive jet ring; 7—nozzle holder; 8—abrasive shutter; 9—tee; 10—sleeve; 11—wheels; 12—air valve; 13—drain valve; 14—inlet valve; 15—manometer; 16—air connection; 17—quick connection.

The setup operates as follows. The abrasive material is poured into the seal through location 2. Close the top of tee 9 through inlet valve 14 to remove parts of the abrasive material. It should be regulated by abrasive shutter 8. Through sleeve 10, we pass the abrasive layer into nozzle 6, in which the speed of the abrasive-recycling mixture will be increased. Nozzle holder 7 is located at the end of sleeve 10 and connected with the nozzle presented in Figure 1 for abrasive jet supply. A special nozzle holder is used, which differs from the traditional one by the fittings for the air supply. Air connection 16 is used to realize air supply, also presented in Figure 1.

The developed nozzle design ensures the organization of the tangential air supply into the nozzle in such a way that the air pushes the abrasive material from the walls. This allows for reducing the wear and increasing the outlet velocity of a mixture.

The operating efficiency of the entire pneumatic abrasive installation immediately depends on the shape and material of the nozzle, which can confirm that this is a key partial installation.

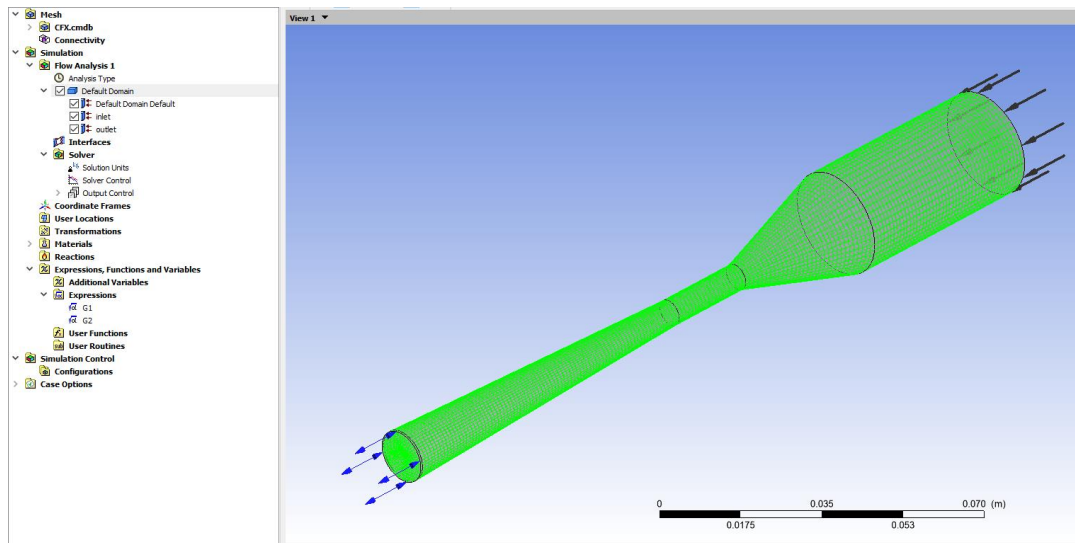
3. Results

3.1. Numerical Simulation Results

Two working phases were considered. The first main phase “fluid” was air. The SST turbulence model for governing equations, as well as the state and the total energy, was chosen. The inlet pressure, temperature, and outlet atmospheric pressure were also set.

The second disperse phase “particle” was river sand with an average diameter of 0.5 mm. The mass flow rate was set. The roughness at the wall was 3.2 μm . The density of the abrasive particles was also specified. The heat exchange was not considered.

The calculation domain, mesh statistics, and convergence of the numerical simulation by mass flow rate \dot{m} are presented in Figure 6.



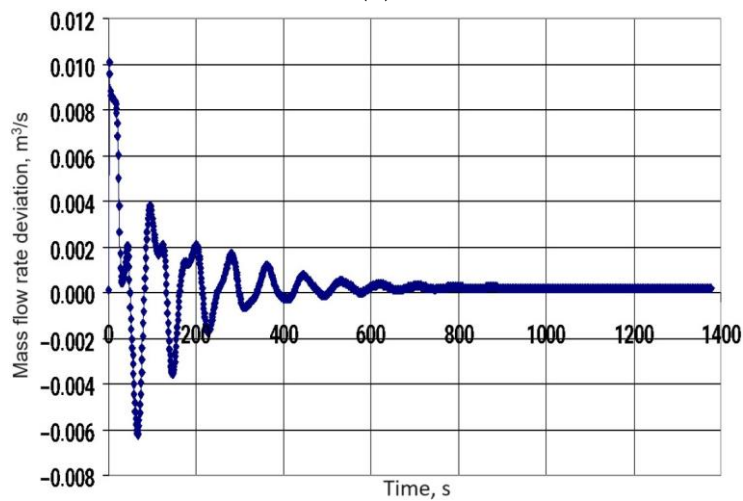
(a)

Mesh Statistics			
Domain Name	Orthog. Angle	Exp. Factor	Aspect Ratio
	Minimum [deg]	Maximum	Maximum
Default Domain	61.0 OK	3 OK	14 OK
Default Domain	0 0 100	0 0 100	0 0 100

Domain Name : Default Domain

Total Number of Nodes = 263700
 Total Number of Elements = 253456
 Total Number of Prisms = 1752
 Total Number of Hexahedrons = 251704
 Total Number of Faces = 21592

(b)



(c)

Figure 6. The calculation domain (a), mesh statistics (b), and convergence of the numerical simulation results (c).

The mesh had the following parameters: the total number of nodes— 2.64×10^5 ; the total number of elements— 2.53×10^5 (including $1.75 \cdot 10^3$ prisms and 2.52×10^5 hexahedrons); the total number of faces— 2.16×10^4 .

The inlet pressure was set. The outlet pressure was atmospheric. Under such conditions, the air consumption was evaluated. Simultaneously, the mass flow rate of the gas–abrasive mixture was calculated as the sum of the mass flow rates of the air and sand particles.

For the chosen model, the time step depends on the convergence of the pressure equations. Therefore, firstly, the time step was set equal to 10% of the machining time; then, it was decreased if there was no convergence.

The operating parameters of the cylindrical nozzle, which are considered to have different geometry, are presented in Table 1.

Table 1. Geometrical and operating parameters of the cylindrical nozzles.

Geometry, m		Mass Flow Rate \dot{m} , kg/s		Velocity, m/s		Mach Number
Diameter d	Length l	Air	Particles	Inlet	Outlet	
0.007	0.044	0.024	0.023	288	453	1.04
0.014	0.044	0.100	0.092	270	481	1.08
0.007	0.004	0.044	0.023	523	794	1.90
0.006	0.022	0.019	0.017	262	470	1.12
0.005	0.022	0.013	0.012	279	463	1.06
0.004	0.022	0.008	0.008	273	457	1.06
0.002	0.022	0.002	0.002	244	466	0.98
0.007 *	0.044	0.053	0.023	637	813	2.27

* nozzle with a perforated insert; the best options are marked in bold.

Table 1 shows that an increase in the nozzle's inner diameter increases its mass flow rate. Also, the average value of the ratio μ is about 1.0.

The last row shows the results for a nozzle equipped with a perforated insert. It has the highest values of the mass flow rate $\dot{m} = 0.023 \text{ kg/m}^3$ and the nozzle's flow ratio $\mu = 2.27$.

The data related to the air flow rate through the nozzle in different nozzle parts (inlet, runway zone end, and outlet) are presented in Table 2.

Table 2. The average flow rates at the runway zone end and the nozzle's outlet, m/s.

Diameter, mm	Runway Zone	Nozzle' Outlet	Runway Zone	Nozzle' Outlet
	ANSYS	FlowVision	ANSYS	FlowVision
6 *	348	352	603	605
7	337	341	581	585
8	330	333	551	555
9	341	345	519	523
10	335	338	483	487
11	340	344	436	440
12	300	305	300	306

* with neglected wear.

The obtained results allow for the study of trends towards a decrease in the air flow rate through the Venturi nozzles and a change in energy efficiency when applying the abrasive jet treatment. The results obtained using different program software (ANSYS and FlowVision) illustrate their convergence.

Under equal conditions, the conical nozzle with a length of 4 mm and external diameter of 15 mm was also calculated. As a result, the technological parameters of the abrasive jet machining gained experimentally with the application of conical nozzles of different cross-sectional areas which are summarized in Table 3.

Table 3. The flow rate of the abrasive jet mixture, kg/h, for different inlet pressures.

Diameter, mm	Inlet Pressure, MPa			
	0.11	0.25	0.54	0.41
3.0	24	30	37	43
4.5	57	71	83	95
6.0	98	124	150	177

The pressure field of the air flow in the nozzle is presented in Figure 7.

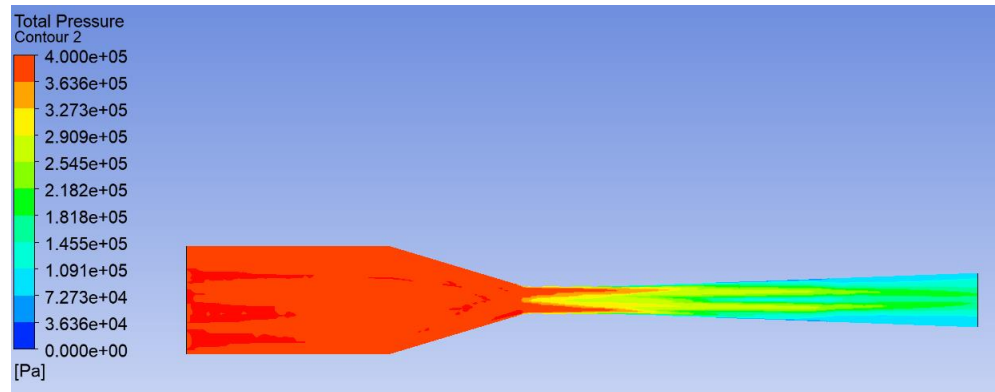


Figure 7. The absolute pressure field of the air flow in the nozzle.

The results of modeling the particle size impact on the velocity distributions in the nozzle UDC 32-450 are presented in Figure 8.

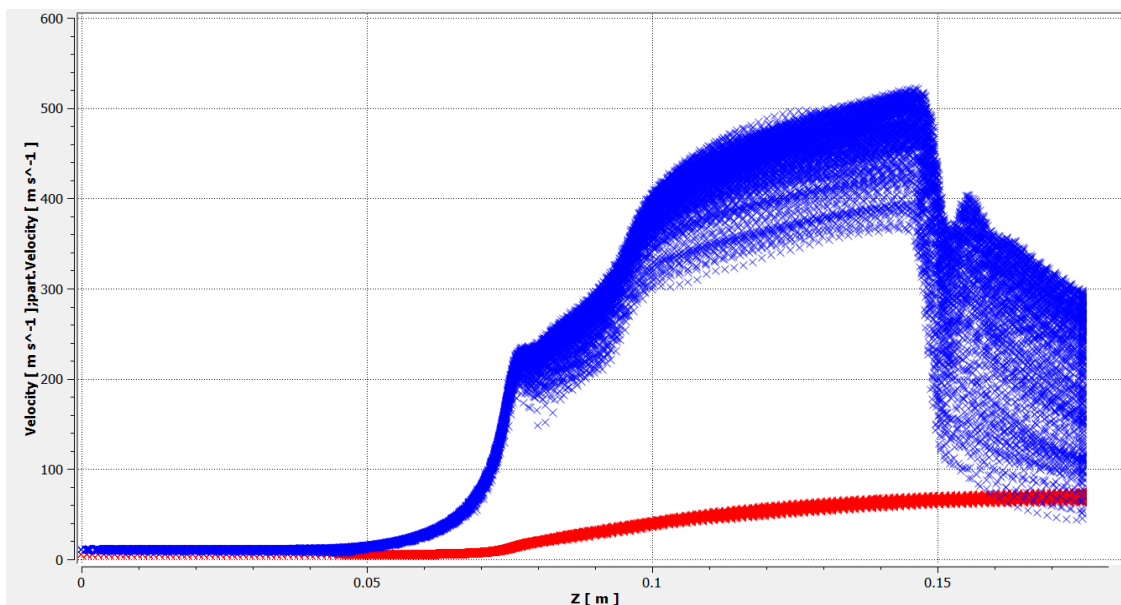


Figure 8. Change in the velocity of air flow (blue) and particles (red) along with the nozzle length.

Particularly, for particles with a 0.5 mm diameter, their mass flow rate was 0.03 kg/s, and the air flow rate was 0.022 kg/s. The velocity of the dispersed phase was much lower than the speed of air. Therefore, the larger the diameter of particles, the lower their velocity. These facts are explained by the differences in the inertial properties.

3.2. Experimental Results Data

The results of the experimental measurements for the cylindrical nozzle with a perforated insert are given in Table 4. It contains the data for the air consumption through the perforated prototype under different pressure values in the receiver.

Table 4. The results of the experimental studies of the cylindrical nozzle with a perforated insert.

Air Pressure in Receiver, MPa	Outflow Time, s	Air Consumption, m ³ /s	Air Pressure in Receiver, MPa	Outflow Time, s	Air Consumption, m ³ /s
0.60–0.58	6	0.00960	0.36–0.34	12	0.00457
0.58–0.56	6	0.00960	0.34–0.32	13	0.00431
0.56–0.54	6	0.00778	0.32–0.30	15	0.00365
0.54–0.52	7	0.00778	0.30–0.28	16	0.00344
0.52–0.50	7	0.00778	0.28–0.26	16	0.00339
0.50–0.48	7	0.00677	0.26–0.24	17	0.00319
0.48–0.46	8	0.00677	0.24–0.22	19	0.00285
0.46–0.44	8	0.00630	0.22–0.20	20	0.00278
0.44–0.42	9	0.00560	0.20–0.18	22	0.00246
0.42–0.40	10	0.00496	0.18–0.16	25	0.00220
0.40–0.38	11	0.00496	0.16–0.14	27	0.00227
0.38–0.36	11	0.00457	0.14–0.12	30	0.00188

The experimentally obtained technological parameters of the abrasive jet machining with the application of the specified nozzle flow areas are summarized in Table 5 and graphically presented in Figure 9.

Table 5. Experimentally obtained technological parameters of abrasive jet machining *.

Nozzle Diameter, mm	Phase	Inlet Pressure, MPa			
		0.11	0.25	0.41	0.54
3.0	Air	0.21	0.27	0.36	0.30
	Sand	24	30	43	37
4.5	Air	0.45	0.60	0.82	0.71
	Sand	57	71	95	83
6.0	Air	0.93	1.13	1.49	1.29
	Sand	98	124	177	150
8.0	Air	1.46	1.80	2.30	2.90
	Sand	181	210	296	370
9.5	Air	2.0	2.4	3.2	4.2
	Sand	246	301	405	503
11.0	Air	2.4	3.1	4.3	6.0
	Sand	339	440	585	720
12.5	Air	3.7	4.2	6.0	7.1
	Sand	451	503	733	908

* air—m³/min; sand—kg/h.

Table 5 and Figure 9 allow the calculations to be made for the related compressor selection and the abrasive material needed for the working nozzle with the specified diameter.

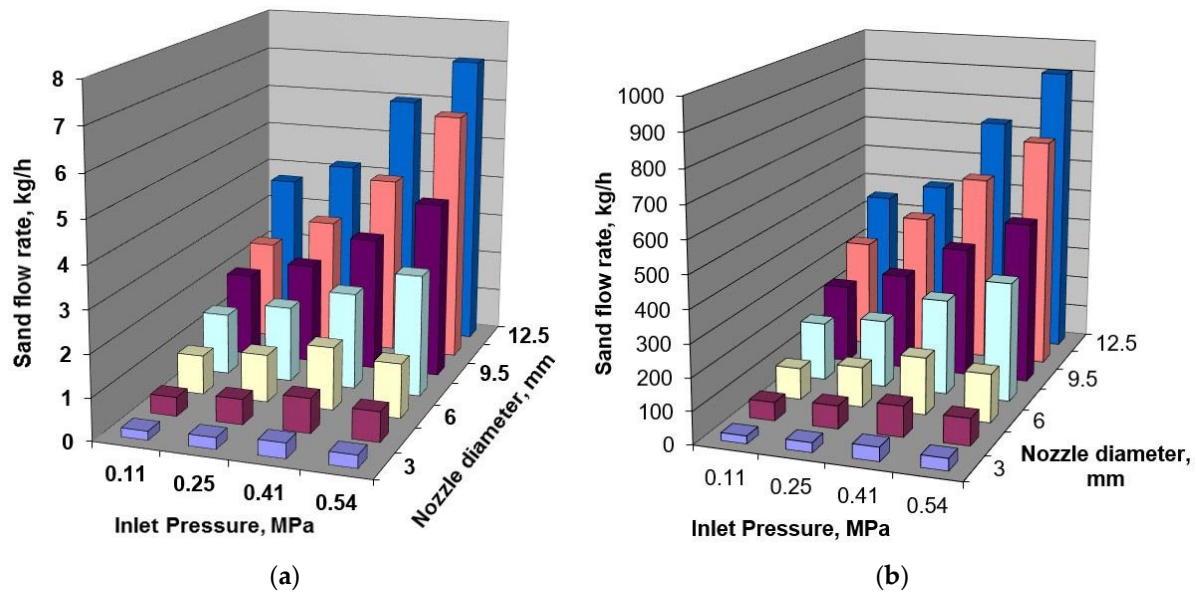


Figure 9. The impact of the nozzle diameter and the inlet pressure on the flow rates: (a) air, m³/min; (b) sand, kg/h.

3.3. Regression Analysis

Under the assumptions that the nozzle's flow ratio μ is proportional to the inlet pressure p_1 ($\mu \sim p_1^\alpha$), for the case of significant pressure differences ($p_1 \gg p_2$), according to Formula (1), the obtained experimental data can be approximated by the following analytical dependence:

$$\dot{m}(p_1) = C p_1^\alpha f \sqrt{\frac{\rho_1}{z} p_1}, \quad (5)$$

where α —the power that reflects the gradient in the impact of the nozzle's flow ratio μ on the mass flow rate \dot{m} ; C —an integral parameter that considers the nozzle's flow ratio μ and the nozzle flow coefficient K :

$$C p_1^\alpha = \mu K. \quad (6)$$

An introduction of the parameters,

$$D = \ln \left(C f \sqrt{\frac{\rho_1}{z}} \right); \beta = \alpha + \frac{1}{2}, \quad (7)$$

allows for simplifying Equation (5) as follows:

$$\dot{m}(p_1) = e^D p_1^\beta. \quad (8)$$

The parameters D and β can be evaluated by the best fit of the experimental data and theoretical dependence. For this purpose, the following root mean squared error (RMSE) should be minimized:

$$RMSE(D, \beta) = \sum_{i=1}^n [D + \beta \ln(p_{1i}) - \ln(\dot{m}_i)]^2 \rightarrow \min, \quad (9)$$

where n —the total number of the experimental dataset; i —the experiment number ($i = 1, 2, \dots, n$); p_{1i} —the i -th measured value of the inlet pressure p_1 , Pa; \dot{m}_i —the i -th measured value of the mass flow rate, kg/s.

The minimizing conditions for the RMSE (9),

$$\begin{cases} \frac{\partial RMSE(D,\beta)}{\partial D} = 2 \sum_{i=1}^n [D + \beta \ln(p_{1i}) - \ln(\dot{m}_i)] = 0; \\ \frac{\partial RMSE(D,\beta)}{\partial \beta} = 2 \sum_{i=1}^n [D + \beta \ln(p_{1i}) - \ln(\dot{m}_i)] \ln(p_{1i}) = 0 \end{cases} \quad (10)$$

allows for obtaining the matrix equation:

$$\begin{bmatrix} n & \sum_{i=1}^n \ln(p_{1i}) \\ \sum_{i=1}^n \ln(p_{1i}) & \sum_{i=1}^n \ln^2(p_{1i}) \end{bmatrix} \begin{Bmatrix} D \\ \beta \end{Bmatrix} = \begin{Bmatrix} \sum_{i=1}^n \ln(\dot{m}_i) \\ \sum_{i=1}^n \ln(p_{1i}) \ln(\dot{m}_i) \end{Bmatrix}, \quad (11)$$

from which the following values of the unknown parameters D and β are obtained:

$$D = \frac{\sum_{i=1}^n \ln(p_{1i}) \cdot \sum_{i=1}^n \ln(p_{1i}) \ln(\dot{m}_i) - \sum_{i=1}^n \ln^2(p_{1i}) \cdot \sum_{i=1}^n \ln(\dot{m}_i)}{[\sum_{i=1}^n \ln(p_{1i})]^2 - n \cdot \sum_{i=1}^n \ln^2(p_{1i})}; \quad (12)$$

$$\beta = \frac{\sum_{i=1}^n \ln(p_{1i}) \cdot \sum_{i=1}^n \ln(\dot{m}_i) - n \cdot \sum_{i=1}^n \ln(p_{1i}) \ln(\dot{m}_i)}{[\sum_{i=1}^n \ln(p_{1i})]^2 - n \cdot \sum_{i=1}^n \ln^2(p_{1i})}. \quad (13)$$

For the experimental points presented in Figure 10, the following values are obtained using Formulas (12) and (13): $D = -6.62$; $\beta = 1.03$.

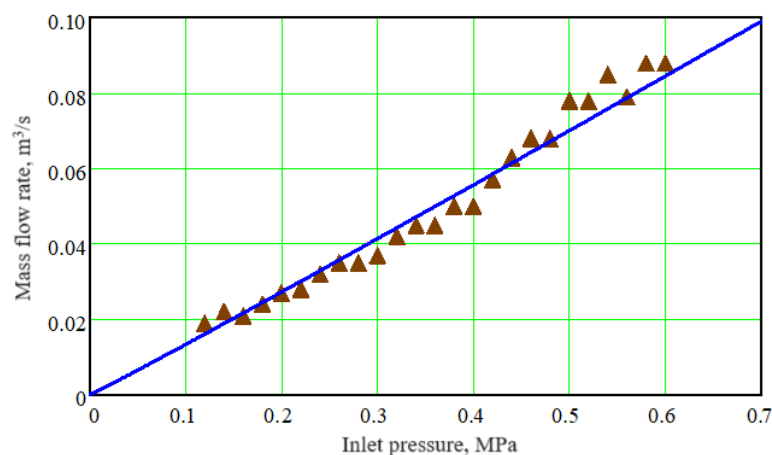


Figure 10. The dependence of the compressed air consumption on its pressure in the receiver: triangles—experimental data; line—approximating curve.

Therefore, after approximation, the dependence (8) of the air consumption can be represented as $\dot{m} = 1.34 \cdot 10^{-3} p_1^{1.03}$. The corresponding approximating curve is presented in Figure 10.

Overall, the organization of the air layer is necessary to reduce the friction of the abrasive against the walls of the nozzle. The option of choosing hydraulically smooth walls can describe the required air layer more thoroughly. In practice, creating this layer requires adjusting the correct air supply because it is essential not to overcompress the main flow, which can lead not to a decrease in friction and vortex formation but to an increase in it and, as a result, negatively affect the operation of the nozzle.

4. Discussion

The results obtained using different software (Table 2) illustrate a good agreement with each other since the discrepancy does not exceed 2%. They also agree with the results presented in [15]. These two facts verify the correctness of the proposed numerical

simulation model chosen to solve the problem, such as studying the two-phase flow through the channels with complicated geometries.

Tables 1–3 prove that an increase in the diameter of nozzles (or runway zone of the Venturi nozzle) causes an increase in the working mixture consumption (air and abrasive material) by more than 4.0 times. Therefore, it is essential not only to decrease the flow slowdown in the nozzle due to friction but also to have a wear-resistant material for its manufacturing.

The receiver volume is equal to 0.23 m^3 , the air pressure is 0.6 MPa, and the length of the air ducts can be neglected as they are short. So, the pressure loss in them is almost non-existent. The research assumes that the air passes through a perforated element of the cylindrical nozzle placed in the unit to determine the pressure drop when the valve is fully open. The reliability of the proposed approach is proven by the fact that the approximation error does not exceed $0.9 \cdot 10^{-4}$, and the average relative error does not exceed 6%.

Overall, all the studies aimed to determine the pressure drop, and the air consumption calculations were performed to describe the properties of the perforated insert. In further computations, they focused on finding the conditions for the air layer formation in the designed fabricated nozzle.

The obtained results will also allow the further improvement of the methodology [21] for the pulsating water jet erosive effect analysis.

During the research of a cylindrical nozzle with an initial length of 22 mm and an internal diameter of 7 mm, it was established that a significant decrease in its length leads to a decrease in the hydraulic resistance of the nozzle. Since the nozzle operates with an abrasive material, reducing the friction of the air–abrasive mixture along with the walls by reducing its length led to a sharp increase in the outlet velocity.

However, the consumption of the compressed air increases disproportionately to the increase in the nozzle's diameter. Often, when the nozzle wears out, there is not a sufficient source of compressed air to ensure the efficiency of the abrasive jet unit. Simultaneously, connecting an additional compressor may not be possible due to the limited characteristics of the electrical network. Therefore, it is impractical to influence the outlet velocity by changing its diameter.

Moreover, the maximum consumption of air and the abrasive material is reached upon reaching the sonic speed. In this case, the operating modes remain unchanged without changing the nozzle's diameter.

Overall, the leading indicators of the nozzle's efficiency are the reactive force of the air–abrasive jet, machining time, penetration depth into the treated surface, and the flow rate. All these indicators increase with an increase in the outlet velocity of the working flow.

The outlet flow velocity depends on the pressure drop and design features of the geometry for the nozzle's flow part. The better geometry of the nozzle is determined by the lower losses due to hydraulic resistance. Since the abrasive particles decrease in the energy of the carrier air flow, it is necessary to organize the maximum velocity at the nozzle outlet.

The maximum flow rate at the outlet also depends on the pressure drop and the inlet temperature. However, the actual velocity will be lower due to the losses. Therefore, the flow ratio has been considered. The flow and loss ratios can also characterize the nozzle efficiency. In this article, the nozzle efficiency was evaluated via the flow ratio and the velocity of the air–abrasive mixture at the nozzle outlet.

Further research will be aimed at studying the impact of the number of holes on the air flow layer formation along with the inner wall and identifying the effect of the particle diameter on the flow rate, considering the heat exchange between the sand, air, and nozzle walls.

5. Conclusions

Based on the results of the CFD modeling of the outflow for the air–abrasive mixture with river sand with an average size of 0.5 mm, it was ascertained that the velocity of the dispersed phase is significantly lower than the velocity of the main phase. Accordingly, the

larger the diameter of the abrasive material, the lower its velocity. It has also been shown that an increase in the mass flow rate of the sand particles decreases the mass flow rate of the air due to the throughput of the nozzle.

It was established that the value of the ratio of the air–abrasive consumption in the nozzle and its flow rate tends to increase disproportionately with the increase in the flow area by 2.0 times, leading to an increase in the flow ratio by 4.5 times.

It was also found that an increase in the nozzle length (up to 4 mm) increased the flow rate by more than two times, increasing the mass mixture consumption and nozzle ratio. Therefore, there appeared to be a possibility of increasing the working efficiency of the abrasive jet machining, e.g., the processing time of a square meter of metal was reduced from 4 min to 2 min while the machining cost is about 5 USD/m² on average.

Applying the throughput inserts resulted in a rise in nozzle efficiency by more than two times. The numerical characteristics of the technological parameters for the abrasive jet treatment were determined experimentally. The mutual discrepancy of the numerical simulation results using the ANSYS and FlowVision did not exceed 2%.

The effective operation term of the proposed nozzle design of about 1000 h corresponds to existing analogs. However, the production cost of the developed nozzle is about USD 20, more than four times less than for available boron carbide nozzles.

Author Contributions: Conceptualization, V.B. and I.P.; methodology, V.B.; software, K.Ž.; validation, I.P. and O.C.; formal analysis, K.Ž.; investigation, V.B., I.P., K.Ž. and O.C.; resources, K.Ž. and O.C.; data curation, I.P.; writing—original draft preparation, V.B. and I.P.; writing—review and editing, K.Ž. and O.C.; visualization, V.B. and I.P.; supervision, O.C.; project administration, V.B. and I.P.; funding acquisition, K.Ž. All authors have read and agreed to the published version of the manuscript.

Funding: This work was supported by the Slovak Research and Development Agency under contract No. APVV-22-0391 and partially funded by the EU NextGenerationEU through the Recovery and Resilience Plan for Slovakia under project No. 09I03-03-V01-00093.

Data Availability Statement: The data presented in this study are available on request from the corresponding author.

Acknowledgments: The research was partially realized within project No. 0124U000636 by the Ministry of Education and Science of Ukraine. The authors also acknowledge the Ulam NAWA Programme (grant no. BPN/ULM/2022/1/00042) for its support while conducting the research.

Conflicts of Interest: The authors declare no conflicts of interest.

References

1. Kun, T.; Wenjie, H.; Yurong, W. Optimization of cold spray nozzles based on the response surface methodology. *J. Eng. Sci.* **2024**, *11*, F1–F11. [[CrossRef](#)]
2. Fesenko, A.; Basova, Y.; Ivanov, V.; Ivanova, M.; Yevsiukova, F.; Gasanov, M. Increasing of equipment efficiency by intensification of technological processes. *Period. Polytech. Mech. Eng.* **2019**, *63*, 67–73. [[CrossRef](#)]
3. Arana-Landín, G.; Uriarte-Gallastegi, N.; Landeta-Manzano, B.; Laskurain-Iturbe, I. The contribution of lean management—Industry 4.0 technologies to improving energy efficiency. *Energies* **2023**, *16*, 2124. [[CrossRef](#)]
4. Rudawska, A.; Danczak, I.; Müller, M.; Valasek, P. The effect of sandblasting on surface properties for adhesion. *Int. J. Adhes. Adhes.* **2016**, *70*, 176–190. [[CrossRef](#)]
5. Pruszczynska, E.; Pietnicki, K.; Klimek, L. Effect of the abrasive blasting treatment on the quality of the pressed ceramics joint for a metal foundation. *Arch. Mater. Sci. Eng.* **2016**, *78*, 17–22. [[CrossRef](#)]
6. Ahmed, F.; Chen, W. Investigation of steam ejector parameters under three optimization algorithm using ANN. *Appl. Therm. Eng.* **2023**, *225*, 120205. [[CrossRef](#)]
7. Yan, J.; Li, Z.; Zhang, H. Investigation on key geometries optimization and effect of variable operating conditions of a transcritical R744 two-phase ejector. *Appl. Therm. Eng.* **2023**, *230*, 120733. [[CrossRef](#)]
8. Xu, Y.; Li, Q.; Li, B.; Guan, Z. Numerical simulation study of hydraulic fracturing nozzle erosion in deep well. *Front. Phys.* **2022**, *10*, 947094. [[CrossRef](#)]
9. Li, A.; Chen, J.; Xi, G.; Huang, Z. Numerical investigation of the effect of primary nozzle geometries on flow structure and ejector performance for optimal design. *J. Mech. Sci. Technol.* **2023**, *37*, 2139–2148. [[CrossRef](#)]
10. Baga, V.M.; Vanyeyev, S.M.; Bondarenko, G.A.; Rodymchenko, T.S. Influence of gas physical properties on labyrinth seals throttling characteristics. *Probl. Reg. Energetics* **2018**, *3*, 83–92.

11. Bañon, F.; Sambruno, A.; Batista, M.; Simonet, B.; Salguero, J. Surface quality and free energy evaluation of S275 steel by shot blasting, abrasive water jet texturing and laser surface texturing. *Metals* **2020**, *10*, 290. [[CrossRef](#)]
12. Aronson, K.E.; Ryabchikov, A.Y.; Zhelonkin, N.V.; Brezgin, D.V.; Demidov, A.L.; Balakin, D.Y. Features of the development and operation of multistage steam jet ejectors. *Therm. Eng.* **2023**, *70*, 245–253. [[CrossRef](#)]
13. Sychuk, V.; Zabolotnyi, O.; McMillan, A. Developing new design and investigating porous nozzles for abrasive jet machine. *Powder Metall. Met. Ceram.* **2015**, *53*, 600–605. [[CrossRef](#)]
14. Heo, S.; Yun, Y.; Jeong, M.; Jee, S. Simulation of supersonic axisymmetric base flow with a data-driven turbulence model. *Aerosp. Sci. Technol.* **2024**, *147*, 109014. [[CrossRef](#)]
15. Baha, V. Improvement of Calculation and Design Methods of Pneumatic Shaft Seals Based on Workflow Simulation. Ph.D. Thesis, Sumy State University, Sumy, Ukraine, 2015.
16. Bondarenko, G.; Baga, V.; Bashlak, I. Flow simulation in a labyrinth seal. *Appl. Mech. Mater.* **2014**, *630*, 234–239. [[CrossRef](#)]
17. Wang, J.; Gong, J.; Kang, X.; Zhao, C.; Hooman, K. Assessment of RANS turbulence models on predicting supercritical heat transfer in highly buoyant horizontal flows. *Case Stud. Therm. Eng.* **2022**, *34*, 102057. [[CrossRef](#)]
18. Bradshaw, P. Turbulent secondary flows. *Annu. Rev. Fluid Mech.* **1987**, *19*, 53–74. [[CrossRef](#)]
19. Kosheleva, O.; Kreinovich, V. Error estimation for indirect measurements: Interval computation problem is (slightly) harder than a similar probabilistic computational problem. *Reliab. Comput.* **1999**, *5*, 81–95. [[CrossRef](#)]
20. Versteeg, H.K.; Malalasekera, W. *An Introduction to Computational Fluid Dynamics: The Finite Volume Method*; Pearson Education: London, UK, 2007.
21. Lehocka, D.; Klich, J.; Pitel, J.; Krejci, L.; Storkan, Z.; Duplakova, D.; Schindlerova, V.; Sajdlerova, I. Analysis of the pulsating water jet maximum erosive effect on stainless steel. In *Advances in Manufacturing II. Volume 4—Mechanical Engineering, Manufacturing 2019*; Springer Nature: Cham, Switzerland, 2019; pp. 233–241. [[CrossRef](#)]

Disclaimer/Publisher’s Note: The statements, opinions and data contained in all publications are solely those of the individual author(s) and contributor(s) and not of MDPI and/or the editor(s). MDPI and/or the editor(s) disclaim responsibility for any injury to people or property resulting from any ideas, methods, instructions or products referred to in the content.